JGR Solid Earth

RESEARCH ARTICLE
10.1029/2021JB021846

Crustal and Upper Mantle Structure Beneath the Southeastern United States From Joint Inversion of Receiver Functions and Rayleigh Wave Dispersion

Qiuyue Yang[1], Kelly H. Liu[1], Tuo Wang[1,2], Jianguo Song[1,3], and Stephen S. Gao[1]

[1]Geology and Geophysics Program, Missouri University of Science and Technology, Rolla, MO, USA, [2]State Key Laboratory of Lithospheric Evolution, Institute of Geology and Geophysics, Chinese Academy of Sciences, Beijing, China, [3]School of Geosciences, China University of Petroleum (East China), Qingdao, China

Key Points:

- Crustal and mantle structure for the top 180 km beneath southeastern U.S. was imaged using receiver functions and Rayleigh wave dispersion
- Results support lower crustal delamination/relamination in the Carolina Terrane and Inner Piedmont of the southern Appalachian Mountains
- High crustal Vp/Vs values observed in the Grenville Province suggest mafic intrusion associated with the Proterozoic Midcontinent rift

Supporting Information:

Supporting Information may be found in the online version of this article.

Correspondence to:

S. S. Gao,
sgao@mst.edu

Citation:

Yang, Q., Liu, K. H., Wang, T., Song, J., & Gao, S. S. (2021). Crustal and upper mantle structure beneath the southeastern United States from joint inversion of receiver functions and Rayleigh wave dispersion. *Journal of Geophysical Research: Solid Earth*, *126*, e2021JB021846. https://doi.org/10.1029/2021JB021846

Received 4 FEB 2021
Accepted 27 SEP 2021

Abstract Using data from 186 stations belonging to the USArray Transportable Array, a three-dimensional shear wave velocity model for the southeastern United States is constructed for the top 180 km by a joint inversion of receiver functions and Rayleigh wave phase velocity dispersion computed from ambient noise and teleseismic earthquake data. The resulting shear wave velocity model and the crustal thickness and Vp/Vs (κ) measurements show a clear spatial correspondence with major surficial geological features. The distinct low velocities observed in the depth range of 0–25 km beneath the eastern Gulf Coastal Plain reflect the thick layer of unconsolidated or poorly consolidated sediments atop the crystalline crust. The low κ (1.70–1.74) and slow lowermost crustal velocities observed beneath the eastern Southern Appalachian Mountains (including the Carolina Terrane and Inner Piedmont) relative to the adjacent Blue Ridge Mountains and Valley and Ridge can be interpreted by lower crustal delamination followed by relamination. The Osceola intrusive complex in the central Suwannee Terrane has similar crustal characteristics as the eastern Southern Appalachian Mountains and thus can similarly be attributed to crustal delamination/relamination processes. The Grenville Province and adjacent areas possess relatively high κ values which can be attributed to mafic intrusion associated with crustal extension in a recently recognized segments of the eastern arm of the Proterozoic Midcontinent Rift.

Plain Language Summary The southeastern United States accommodates some of the most diverse geological features in the world, as a result of several episodes of continental rifting, formation of ocean basins, and continental collision over the past several billion years. Imaging the interior structure in the area provides key information needed for better understanding how the Earth has operated and evolved over its history. In this study we use ground vibrations generated by distant earthquakes and ambient noise to image the structure in the top 180 km beneath the Southern Appalachian Mountains and the bordering coastal plains. The observations suggest that the eastern part of the Southern Appalachian Mountains, including the Carolina Terrane and the Inner Piedmont, may have lost its original lower part of the crust which has been replaced by a layer of more felsic (i.e., rich in silicate minerals) materials derived from the mantle. The measurements also support a recently proposed model that the Midcontinent Rift could have extended more southward than previously thought, and provide some intriguing preliminary observations for additional investigations, such as the low mantle velocities and their possible linkage with an area of thinner than normal lithosphere in northern Florida.

1. Introduction

The Southern Appalachian Mountains (SAM) of the southeastern United States (SEUS) are bordered by the Atlantic Coastal Plain to its southeast and the Gulf Coastal Plain to its south (Figure 1). The SAM and adjacent areas have undergone two complete Wilson cycles (Thomas, 2006), including the assembly of Rodinia (1.35–1.1 Ga) followed by the opening of the Iapetus Ocean (760–530 Ma), and the assembly of Pangaea (350–300 Ma) followed by the opening of the Atlantic Ocean (~180 Ma). Such a tectonic complexity makes the area an ideal location to study modifications of the crust and upper mantle by a variety of tectonic processes including continental rifting, passive margin evolution, plate subduction, and continental collision.

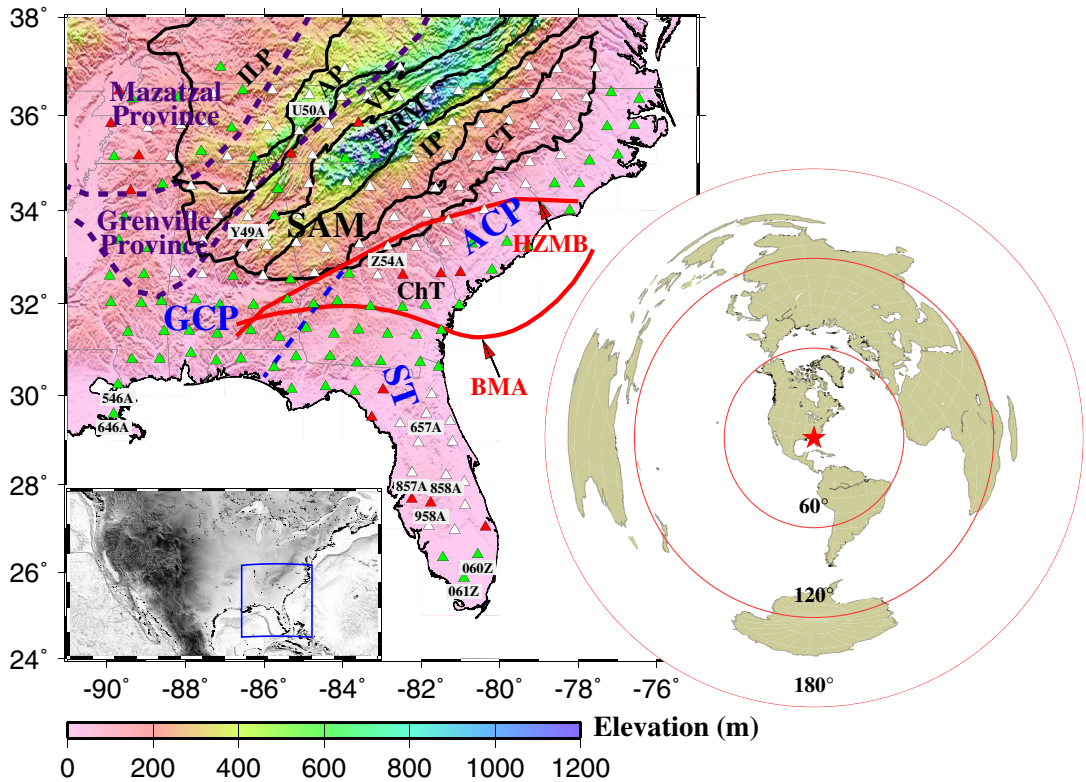

Figure 1. Elevation map showing seismic stations used in the study (triangles) and major tectonic provinces (Thomas, 2006). The blue dashed line represents the boundary between the Gulf Coastal Plain and the Atlantic Coastal Plain, and the two purple dashed lines outline the Grenville and Mazatzal provinces. White triangles represent stations in Group A, red ones for Group B, and green ones for Group C. Named stations are those mentioned in the main text. The inset in the lower right corner is an azimuthal equidistant projection map centered at the study area showing the distribution of earthquakes used for RF (green circles) and TS (blue circles) analyses. The rectangle area in the inset map in the lower left corner shows the location of the study area. ACP: Atlantic Coastal Plain; AP: Appalachian Plateau; BMA: Brunswick Magnetic Anomaly; BRM: Blue Ridge Mountains; ChT: Charleston Terrane; CT: Carolina Terrane; GCP: Gulf Coastal Plain; HZMB: Higgins-Zietz Magnetic Boundary; ILP: Interior Low Plateau; IP: Inner Piedmont; SAM: Southern Appalachian Mountains; ST: Suwannee Terrane; VR: Valley and Ridge.

1.1. Geological Setting

During the final phase of the Grenville orogeny (1.35–1.1 Ga), the Grenville terranes accreted onto Laurentia along a southeast-trend convergent margin (Figure 1), leading to the assembly of the supercontinent Rodinia (Loewy et al., 2003; Thomas, 2006; Tohver et al., 2004; Whitmeyer & Karlstrom, 2007). The supercontinent rifted at ~570 Ma along the eastern margin of Laurentia and resulted in the opening of the Iapetus Ocean (Rogers & Santosh, 2003; Thomas, 2006). Rift-related igneous intrusions are suggested to exist in the crust beneath the SAM (Aleinikoff et al., 1995; Owens & Tucker, 2003). A volcanic island arc, the Carolina Terrane (Figure 1), accreted onto the Inner Piedmont and formed the Central Piedmont Suture after the opening of the Iapetus Ocean and prior to the assembly of Pangaea (Dennis & Wright, 1997; Hawman et al., 2012). To the northwest of the Inner Piedmont lies the high-elevation Blue Ridge Mountains with a root of thickened crust (Hopper et al., 2016). Besides the buoyancy of the crustal root, a low-velocity zone in the upper mantle beneath the Blue Ridge Mountains could also be a source of positive buoyancy to support the high topography (MacDougall et al., 2015).

The Alleghanian Orogeny (325–260 Ma) is believed to be the most recent orogenic activity in eastern U.S. (Hatcher et al., 1989; Pollitz & Mooney, 2016), which completed the assembly of the supercontinent Pangaea (Iverson & Smithson, 1983). It is generally accepted that Pangaea was formed by the collision of Gondwana and Laurentia, but the location of the suture of the two continents in the SEUS is debated. While some previous studies suggest that the suture is represented by the Brunswick Magnetic Anomaly (Heatherington

& Mueller, 2003; McBride & Nelson, 1988; Nelson et al., 1985) (Figure 1), more recent investigations advocate that the magnetic anomaly represents an intra-Gondwanan linear structure and the Gondwana/Laurentia suture is located further north, probably represented by the Higgins-Zietz Magnetic Boundary (Boote & Knapp, 2016; Higgins & Zietz, 1983; Hopper et al., 2017; Marzen et al., 2019) (Figure 1). The breakup of Pangaea started in the Middle to Late Triassic, which developed rift basins across Georgia (McBride, 1991) and along the east coast (Schlische, 1993), creating the extensive basaltic magmatism of the Central Atlantic Magmatic Province at ~190 Ma (Marzoli et al., 1999; Whalen et al., 2015).

1.2. Previous Seismic Investigations of Lithospheric Structure Beneath the SEUS

The crustal and mantle structure of the SEUS has been investigated by numerous geoscientific techniques over the past several decades, with vastly different spatial coverage and resolution. In the following we briefly summarize seismic tomography and receiver function (RF) results that are most relevant to the present study, with an emphasis on those using the USArray passive source seismic data. Some of the recent continental-scale studies that cover the SEUS are also briefly discussed.

1.2.1. Southern Appalachian Mountains

Pn tomography and Rayleigh wave dispersion and RF joint inversion studies (Buehler & Shearer, 2017; Shen & Ritzwoller, 2016) utilizing data from the USArray reveal a southeastward thinning of the crust across the SAM, a feature that has been pervasively observed by numerous passive or active source seismic investigations (see below) and is consistent with the seaward decrease in elevation and increase in Bouguer gravity anomalies (Zhang et al., 2020). Depending on the assumed crustal velocities, the estimated crustal thickness (H) can differ by up to 5 km in the SEUS (Buehler & Shearer, 2017). Along a NW-SE trending profile across the SAM, a waveform migration study (Hopper et al., 2016) reveals that the Blue Ridge Mountains possess the thickest crust, ~52 km, which is greater than that found using Pn tomography (Buehler & Shearer, 2017). H measured by the majority of reflection/refraction and RF studies ranges from ~36 to 55 km within the SAM, ~36–37 km for the Carolina Terrane, 50–55 km for the Blue Ridge Mountains, 50 km for the Valley and Ridge, and 55 km for the Appalachian Plateau and the Interior Low Plateaus (Buehler & Shearer, 2017; Hawman et al., 2012; Kean & Long, 1980; Li et al., 2020; Ma & Lowry, 2017; Parker et al., 2013; Prodehl et al., 1984; Shen & Ritzwoller, 2016; Verellen et al., 2020; Wagner et al., 2018). The high H values beneath the Blue Ridge Mountains are explained by the combined result of the Alleghanian thrust loading and the inherited thickened crust from continental collision during the Proterozoic Grenville orogeny (Parker et al., 2013).

Crustal Vp/Vs (κ) values that are lower than the typical bulk crustal κ of 1.78 (Christensen, 1996) are observed in the Carolina Terrane and the Inner Piedmont (Hawman et al., 2012; Ma & Lowry, 2017; Parker et al., 2013; Zhang et al., 2020), and a crustal delamination/relamination hypothesis is proposed to explain the low κ measurements (Parker et al., 2013). Overall, the Appalachian Mountains show some of the highest crustal shear velocities in the continental United States (e.g., Porter et al., 2016; Shen & Ritzwoller, 2016), an observation that is consistent with the hypothesis that crustal densities increase beneath older mountain ranges (Fischer, 2002).

The Grenville Terrane is bounded by two low-velocity anomalies in the upper mantle, the Atlantic Coastal Plain to the east and the Suwannee Terrane to the south, respectively (Netto & Pulliam, 2020). Along the Grenville Province and a narrow zone to its east, which is recently proposed as an extension of the eastern arm of the Proterozoic Midcontinent Rift (Stein et al., 2018), distinct low velocity anomalies are found in the crust, probably caused by thick sediments and volcanic rocks (Wang, Zhao, et al., 2019). Comparing with the surrounding areas, a relatively thin crust of ~40 km beneath the New Madrid Seismic Zone in the Mazatzal Province on the northwestern corner of the study area is observed, suggesting the existence of a zone of weakness (Liu et al., 2017; McGlannan & Gilbert, 2016). Positive gravity anomalies there indicate that the high-density crust may play an important role in maintaining the low elevations (Liu et al., 2017; McGlannan & Gilbert, 2016).

1.2.2. Coastal Plains and the Suwannee Terrane

Surface wave tomography studies (e.g., Bensen et al., 2008; Gaite et al., 2012; Porter et al., 2016; Spica et al., 2016) image low velocity anomalies in the upper crust beneath the Gulf Coastal Plain, which are attributed to the thick sediments (up to 10 km thick, Laske & Masters, 1997). RF and seismic tomography studies indicate that compared with the SAM, the Atlantic and Gulf of Mexico coastal plains possess relatively thin crust, in the range of ~25–35 km (Buehler & Shearer, 2017; Li et al., 2020; Liu & Shearer, 2021; Ma & Lowry, 2017; Shen & Ritzwoller, 2016). With the exception of the central Suwannee Terrane, the observed κ values in the coastal plains and most part of the Suwannee Terrane are generally greater than 1.80 (Ma & Lowry, 2017), which are higher than the global average value of 1.78 for continental crust (Christensen, 1996) and thus may indicate a mafic composition. The overall mafic crustal composition of the Atlantic Coastal Plain is commonly attributed to the Central Atlantic Magmatic Province formed during the early stage of the formation of the passive margin (Marzoli et al., 1999; Nomade et al., 2007; Whalen et al., 2015).

Using data provided by the EarthScope USArray Transportable Array (TA) stations, Yuan et al. (2014) construct a 3-D shear wave velocity model of the lithosphere and asthenosphere in the continental U.S. They observe high velocities northwest of the Suwannee Terrane in Florida and beyond the coastline persisting down to the uppermost mantle to a depth of about 150 km, indicating that the exotic terranes extend into the lithosphere. The study proposes that deep-rooted (>150 km) high-velocity blocks east of the continental rift margin represent the Gondwanian terranes of Pan-African affinity. This high velocity anomaly is also revealed by another 3-D shear wave velocity model in the uppermost mantle (Shen & Ritzwoller, 2016). Moving deeper, a 3-D seismic velocity model of the upper mantle (85–460 km) for the southern U.S. recently constructed by Netto and Pulliam (2020) suggests a high-velocity anomaly extending from ~100 to ~450 km deep beneath the northern Suwannee Terrane, which seems to be associated with the Suwannee-Wiggins Suture Zone (Netto & Pulliam, 2020). To the south of this high velocity zone, in central and northern Florida, low seismic velocities in the upper mantle are observed by several tomography studies, extending deeper than 180 km (Biryol et al., 2016; Golos et al., 2020; Netto & Pulliam, 2020; Pollitz & Mooney, 2016; Schmandt & Lin, 2014; Wagner et al., 2018).

A recent seismic body-wave attenuation study (Shrivastava et al., 2021) finds a zone of low attenuation (i.e., high Q) in the Gulf Coastal Plain. The center of the low attenuation layer is estimated to be at the depth of ~70 km using a modified version of the spatial coherency analysis procedure (Gao & Liu, 2012). The spatial distribution of the low attenuation measurements is consistent with a high velocity zone revealed by seismic tomography studies (e.g., Golos et al., 2020). Remnant lithospheric segments in the lower crust and upper mantle are suggested based on the attenuation measurements (Shrivastava et al., 2021).

1.3. Significance of the Present Study

Due to the influence of thick sedimentary layers atop the crust in the Atlantic and Gulf coastal plains, it is difficult to reliably image crustal and upper-mantle structure using RF analysis or surface wave tomography alone, leading to occasionally conflicting crustal thickness and lithospheric velocity measurements. Additionally, many of the recent studies on crustal and upper mantle properties either target the entire contiguous United States (e.g., Buehler & Shearer, 2017; Liu & Shearer, 2021; Ma & Lowry, 2017; Shen & Ritzwoller, 2016; Yuan et al., 2014), or along densely spaced profiles (e.g., Hopper et al., 2016; Li et al., 2020; MacDougall et al., 2015; Parker et al., 2013; Verellen et al., 2020). There are only a limited number of post-USArray studies on crustal and mantle structure focusing on the SEUS (e.g., Biryol et al., 2016; Hopper et al., 2017; Wagner et al., 2018), among which none has used the RF and Rayleigh wave dispersion joint inversion technique that this study employs.

Our strategy is to use a non-linear Monte Carlo joint inversion of RFs and Rayleigh wave phase velocities (Shen et al., 2013) at stations that could provide reliable RF measurements, while for stations that could not provide reliable RF measurements, we invert the Rayleigh wave phase velocities using H and κ values from global models for generating initial inversion models. The joint inversion analysis can result in more reliably determined shear wave velocities compared with surface wave tomography and more accurate H measurements compared with RF approaches. H-κ stacking RF analysis (Zhu & Kanamori, 2000) is utilized

to provide stacked RF time series and H and κ measurements. Strong reverberations produced by the unconsolidated sediments atop the crust may mask the converted phases from the Moho, leading to erroneous H and κ measurements (Yu et al., 2015; Zelt & Ellis, 1999). To better constrain our RF measurements, a deconvolution-based reverberation-removal technique (Yu et al., 2015) is applied on the original RFs to remove or significantly reduce the reverberation effects. For Rayleigh wave phase velocity dispersions at short periods (6–24 s), ambient seismic noise tomography (Yao et al., 2006) is used to obtain phase velocities at different periods. For Rayleigh wave phase velocity dispersions at long periods (28–120 s), two-station (TS) analysis (Yao et al., 2006) is applied to extract phase velocities from teleseismic data. Tectonic implications of the study area, including delamination/relamination beneath the eastern SAM and magmatic intrusion beneath the Grenville Province in SEUS, have been proposed by either H and κ evidence or seismic velocity variations (e.g., Behrendt et al., 1990; Parker et al., 2013). Our study provides more comprehensive interpretations by combining the two. Additionally, several previously unrecognized features, e.g., crustal delamination/relamination beneath the Suwannee Terrene, are suggested by our joint investigation of multiple properties of the crust and uppermost mantle.

2. Data and Methods

2.1. Data

Broadband seismic data recorded by 186 USArray TA stations were obtained from the Incorporated Research Institutions for Seismology (IRIS) Data Management Center (DMC) within the range of 76°–90°W, and 25°–37°N (Figure 1). For ambient noise tomography, broadband waveforms with a one-day length (86,400 s) were requested. Because our objective is to measure Rayleigh wave phase velocities, only the vertical component waveforms were selected. Subsequently, all the seismograms were uniformly resampled to 5 Hz. To obtain Rayleigh wave phase velocity measurements from the TS approach, we requested broadband seismic data from 1,351 earthquakes with a minimum body wave magnitude (M_b) equal to or greater than 5.7 (Figure 1). The seismograms were then resampled to one sample per second for future data processing.

To compute RFs, data from 936 teleseismic events in the epicentral distance range 30°–180° were requested from the IRIS DMC (Figure 1). The cutoff magnitude (M_c) is constrained by $M_c = 5.2 + (\Delta - \Delta_{min})/(\Delta_{max} - \Delta_{min}) - D/D_{max}$, where Δ is the epicentral distance in degrees, D is the focal depth in kilometers, $\Delta_{min} = 30°$, $\Delta_{max} = 180°$, and $D_{max} = 700$ km (Liu & Gao, 2010). A total of 13,099 three-component seismograms were obtained and windowed from negative 5 s to positive 50 s relative to the theoretical first P-wave arrival computed using the IASP91 model (Kennett & Engdahl, 1991).

2.2. Methods

2.2.1. Surface Wave Phase Velocity and RF Data Processing

Rayleigh wave phase velocity dispersion measurements are obtained from both ambient seismic noise and teleseismic events. The empirical Green's function (EGF) analysis is applied to extract dispersion measurements at short periods (6–24 s) from ambient noise. The four main steps for the EGF analysis include single station preprocessing to obtain ambient noise data, cross-correlation and temporal stacking to provide enhanced EGFs (see example of cross-correlation in Figure 2), dispersion curve selection to discard unreliable measurements, and phase velocity inversion to obtain phase velocity maps at different periods from 1-D dispersion curves (e.g., Wang, Feng, et al., 2019; Wang, Gao, et al., 2019). To extract long-period (28–120 s) Rayleigh wave phase velocity dispersion measurements, we apply the TS analysis (Yao et al., 2006). A multiple filter technique (Dziewonski et al., 1969) and an image transformation technique (Yao et al., 2006) are used to provide long-period dispersion curves for manual checking. Finally, phase velocity images are obtained from 6 to 24 s with an interval of 2 s and 28–120 s with an interval of 4 s (e.g., Yang et al., 2008; Yao et al., 2006). For all periods, the grid dimension is 0.4° × 0.4° with a sampling step of 0.1°. Figure 3 shows phase velocity maps at different periods.

For processing RF data, we firstly enhance the signals by applying a 4-pole, 2-pass Bessel band pass filter (0.06–1.2 Hz) on all the obtained seismograms, and only teleseismic events with a signal-to-noise ratio

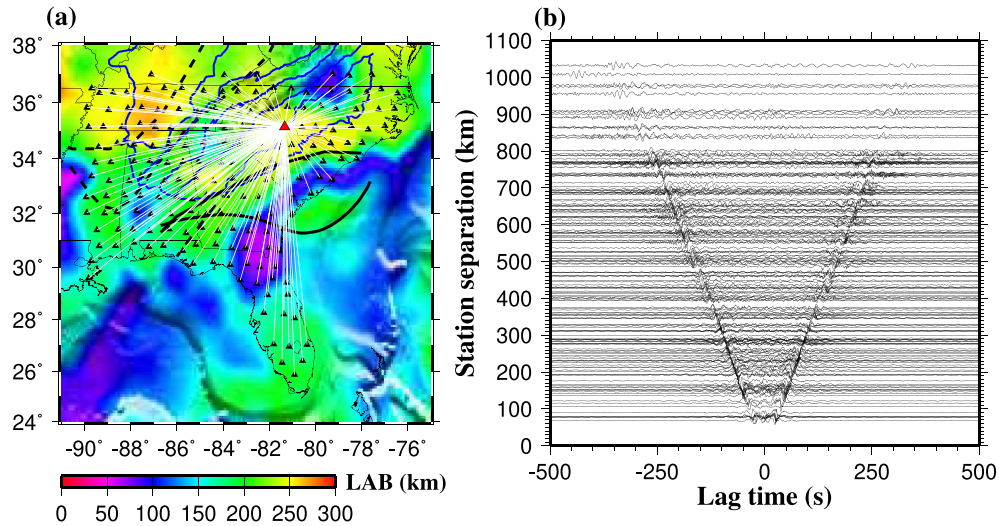

Figure 2. (a) Raypaths (white lines) between Station KMSC (red triangle) and other stations (black triangles). The background image shows the depth of the lithosphere-asthenosphere boundary (Pasyanos et al., 2014). (b) 2–40 s band-pass filtered cross-correlation functions between Station KMSC and other stations.

(SNR) greater than 4.0 are retained (e.g., Gao & Liu, 2014). A frequency domain water-level deconvolution procedure (Ammon et al., 1990; Clayton & Wiggins, 1976) is applied on the filtered seismograms to deconvolve the vertical component from the radial component. Next, the H-κ stacking procedure (Zhu & Kanamori, 2000) is applied to determine the optimal H and κ measurements with the weighting factors for the *PmS*, *PPmS*, and *PSmS* phases of 0.5, 0.3, and 0.2, respectively (Nair et al., 2006). We use a 10-iteration bootstrap resampling approach (Efron & Tibshirani, 1986) to compute the average H and κ values.

Due to the thick sedimentary layer in the coastal plain region, strong reverberations caused by this low density and low velocity layer may mask the P-to-S converted phases (*PmS* and multiples) on the seismograms, leading to erroneous H and κ measurements (Cunningham & Lekic, 2019, 2020; Langston, 2011; Yu et al., 2015; Zelt & Ellis, 1999). In this study we use a resonance-removal filter in the frequency domain (Yu et al., 2015) to remove or significantly reduce the reverberations. The amplitude (r_0) and the time delay (Δt) of the first trough on the RF autocorrelation functions are used to generate the filters. Figure 4 shows two examples of H-κ RF stacking from Station X53A and Station Y59A. The latter is processed with the resonance-removal filter.

We classify all the stations into three groups according to the quality of stacked RFs. Group A is for stations with a clear *PmS* phase and a well-defined maximum stacking amplitude on the H-κ plot. Group B is for stations that have multiple possible H-κ pairs, and the optimal H and κ values are determined by comparing results from adjacent stations. Group C is for stations that have an inadequate number of high-quality RFs (less than 5) or have low quality RFs that could not lead to reliable H and κ values. A total of 92 seismic stations belong to Group A, 14 to Group B, and 80 to Group C (Figure 1).

2.2.2. Joint Monte Carlo Inversion

We adopt a non-linear Bayesian Monte Carlo joint inversion of RFs and Rayleigh wave phase velocity dispersion (Shen et al., 2013) to construct a high-resolution 3-D shear wave velocity model for the top 180 km beneath the SEUS. A 3-D initial model is generated using the H and κ values derived from the H-κ stacking analysis or other *a priori* constraints, with a 25% allowable perturbation for the H values. The initial model is divided into two layers to respectively represent the crystalline crust (from the surface to H) and the upper mantle (from H to 180 km). A 4 cubic B-spline interpolation and a 5 cubic B-spline interpolation of the IASP91 model (Kennett & Engdahl, 1991) are applied to the crustal and upper mantle layers, respectively. The allowed magnitude of perturbation for the 9 velocity coefficients is 20%. For Group A stations, we use the RF traces and the resulting H and κ values from H-κ stacking for the joint inversion (i.e., Station X53A, Figures 5b–5d). For stations in Group B, we only invert the phase velocities due to the unclear *PmS* phases

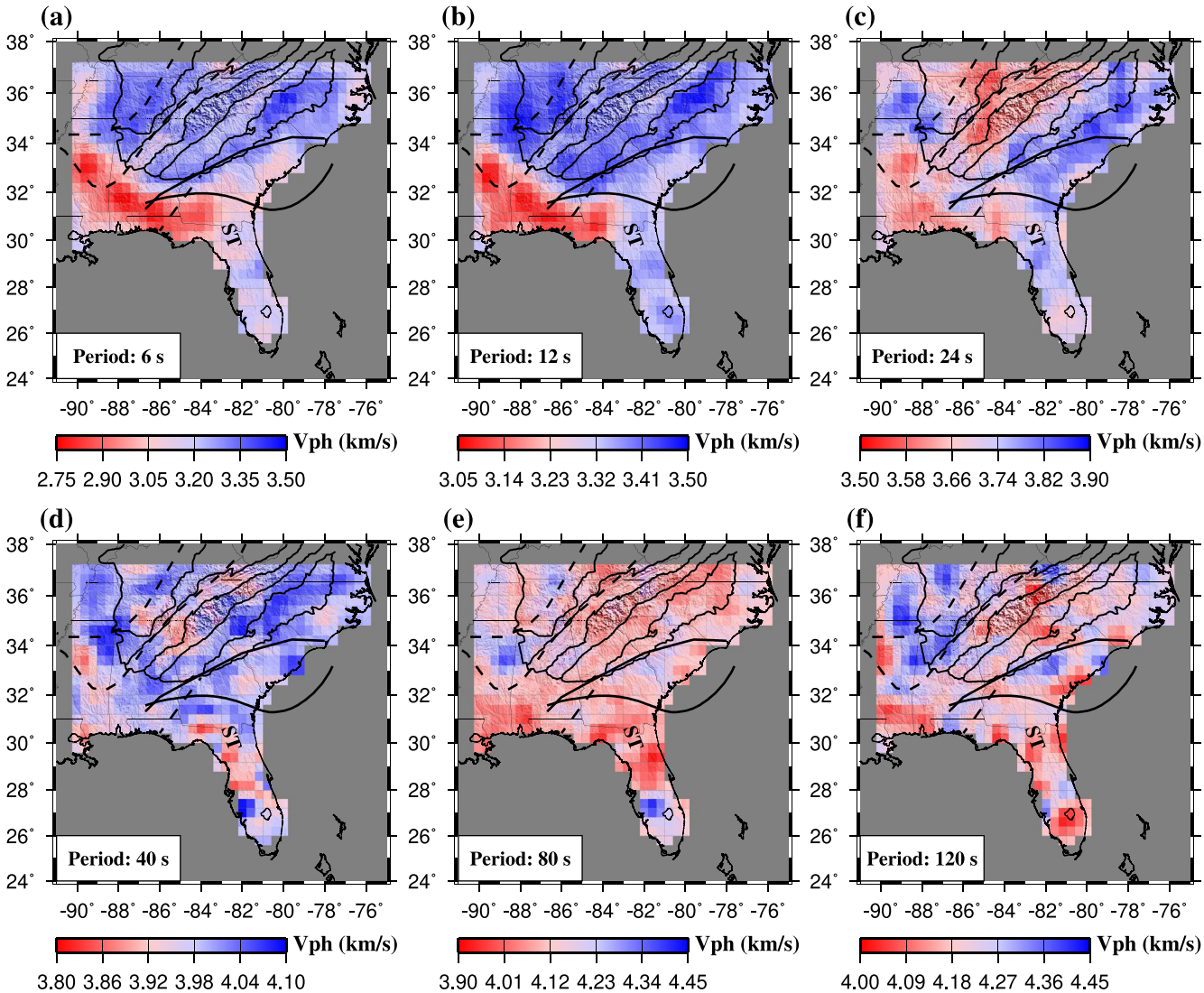

Figure 3. Rayleigh wave phase velocity maps from EGF (a–c) and TS (d–f) analyses. (a) 6 s (b) 12 s (c) 24 s (d) 40 s (e) 80 s (f) 120 s.

on RFs, and use the H and κ values to construct the initial model (i.e., Station 555A, Figures 5e and 5f). For Group C stations, we use the H values provided by the CRUST1.0 global model (Laske et al., 2013) and a fixed κ value of 1.78 (Christensen, 1996) to construct the initial model and to invert phase velocities (i.e., Station W44A, Figures 5g and 5h). Because κ values derived from the H-κ stacking method can only reflect the averaged value in the crust, we use a fixed κ of 1.75 for the uppermost mantle (e.g., Shen et al., 2013; Wang, Gao, et al., 2019).

To make physical dispersion corrections (Kanamori & Anderson, 1977), we use Q values from the PREM model (Dziewonski & Anderson, 1981). Three thousand iterations are adopted to reject unreliable inverted shear wave velocity values using a combined root mean square misfit function for Rayleigh wave phase velocity dispersion and RF measurements. The combined RMS misfit function can be expressed by $\chi^{\text{joint}} = 0.5\left(\frac{\chi^{\text{SW}}}{\chi^{\text{SW}}_{\text{min}}} + \frac{\chi^{\text{RF}}}{\chi^{\text{RF}}_{\text{min}}}\right)$, where χ^{SW} and χ^{RF} are the RMS misfits for surface wave dispersion and RFs, respectively, and $\chi^{\text{SW}}_{\text{min}}$ and $\chi^{\text{RF}}_{\text{min}}$ represent the defined corresponding minimum values (e.g., Shen et al., 2013).

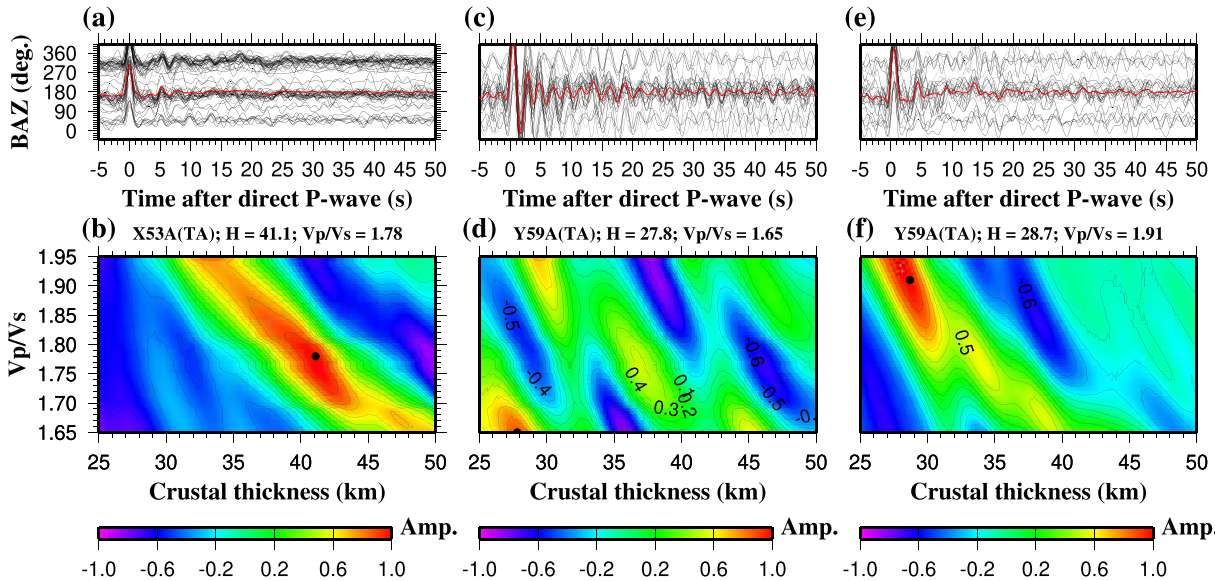

Figure 4. (a) Original RFs from Station X53A plotted against the back azimuth (BAZ). The black traces represent individual RFs, and the red trace is the result of simple time domain summation of the individual traces. (b) H-κ plot using the RFs in (a). (c) Same as (a), but for Station Y59A. Reverberation are clearly observed on the stacked RF (red trace). (d) H-κ plot using the RFs in (c). (e and f) are the same as (c and d), but after removing the reverberations from the RFs using the approach of Yu et al. (2015).

3. Results

3.1. Phase Velocity Maps and Resolution Test

The selected Rayleigh wave phase velocity dispersion curves are inverted to construct phase velocity maps at different periods. At the periods of 6 and 12 s (Figures 3a and 3b), relatively high phase velocities (~3.3 km/s and ~3.4 km/s, respectively, for $T = 6$ s and $T = 12$ s) are observed within the SAM and parts of the Suwannee Terrene. The Gulf Coastal Plain is characterized by relatively low phase velocities (~2.8 and 3.1 km/s) at these periods. At the period of 24 s (Figure 3c), phase velocities within the SAM (~3.6 km/s), with the exception of the Carolina Terrane, are lower than those in the Atlantic Coastal Plain (~3.8 km/s), and phase velocities beneath the Gulf Coastal Plain are comparable with those observed in the SAM. At the period of 40 s (Figure 3d), phase velocities within the SAM become more consistent with those outside the region, and the central part of the SAM (the Appalachian Plateau and the Valley and Ridge) shows low phase velocities relative to the surrounding areas. The central and northwestern portions of the Suwannee Terrane are also characterized by relatively low velocities at this period (Figure 3d). At the periods of 80 and 120 s (Figures 3e and 3f), the Mazatzal Province and Grenville Province in the northwestern corner of the study area show the highest phase velocities in the entire study area.

We utilize a standard checkerboard resolution test to check the reliability of the observed phase velocities. Figure S1 in Supporting Information S1 shows the testing results at 6 example periods (6, 12, 24, 40, 80, and 120 s). We synthesize a target model with alternating positive and negative 5% perturbation velocities relative to 4 km/s with the grid dimension of 1.5° × 1.5°. Using exactly the same data and inversion procedures as those used in the real data set, we obtain recovered velocity models at different periods (Figures S1b–S1g in Supporting Information S1). Except for the southern tip of the Suwannee Terrane, well-reconstructed pattern and magnitude are obtained for all the periods.

3.2. κ Measurements From RFs

The κ values obtained from the H-κ stacking analysis range from 1.70 at Station Z54A located near the southeastern boundary between the SAM and Atlantic Coastal Plain to 1.94 at Station 657A in the northern part of the Suwannee Terrene, with a mean value of 1.82 ± 0.05 for the entire study area (Figure 6). The Grenville Province within the SAM is characterized by relatively high κ values compared with the rest of

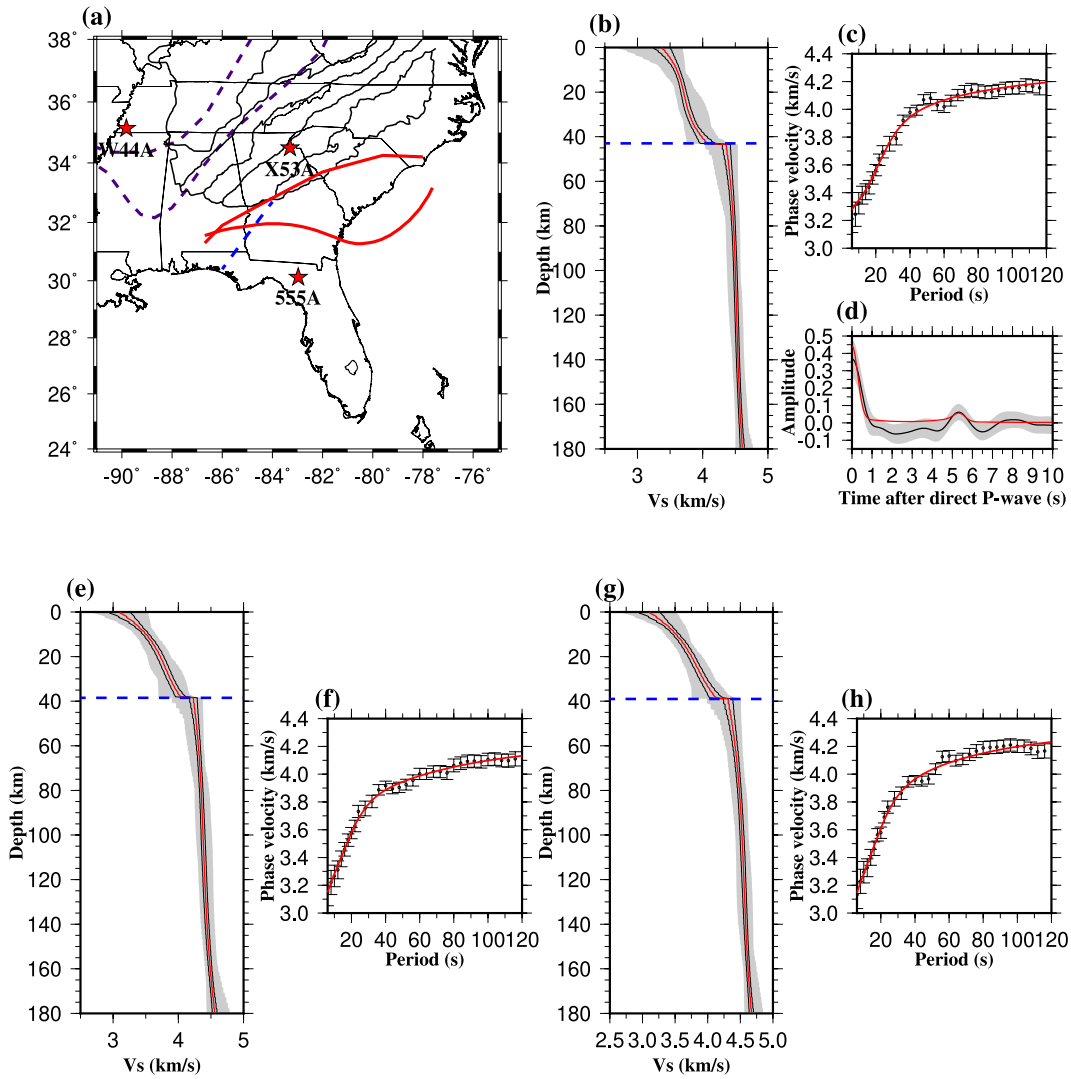

Figure 5. Inversion results of three seismic stations from different groups. (a) Station location map. Red stars indicate the locations of the three stations. (b–d) Joint inversion results for Station X53A from Group A. (e–f) are for Station 555A from Group B, and (g–h) are for Station W44A from Group C. (b, e, and g) are ensembles of accepted shear velocity models. Light gray area represents the full width of the ensemble, and the 1σ width of the ensemble under the assumption of Gaussian distribution is enclosed by the two black curves. The red curve is the mean of all the accepted shear velocity models. The Moho beneath the station is indicated by the horizontal blue dashed line. (c and f) are observed Rayleigh wave phase velocities (black dots) and 1σ error bars. The red curve is the prediction from the best fitting model. (d) Stacked RF (black curve) and the 1σ uncertainty (light gray area). The red curve is the predicted RF from the best fitting model in (b). Note that the procedure that we used does not attempt to fit the entire RF, but only the amplitude and arrival time of the *PmS* phase.

the SAM, and the mean κ value computed over the 15 stations within the Grenville Province is 1.85 ± 0.03. There is a sharp boundary in the κ observations between the southeastern SAM and the Atlantic Coastal Plain (Figure 6). With the exception of the central part of the Suwannee Terrane, which is a low-κ zone (e.g., 1.72 at Station 857A, 1.73 at Station 858A, and 1.72 at Station 958A), the entire coastal plain possesses relatively high κ measurements. The Higgins-Zietz Magnetic Boundary separates an area of high κ to the south where the values are comparable to those in the northern Suwannee Terrane, and an area of low κ to the north where the measurements are similar to those observed in the SAM.

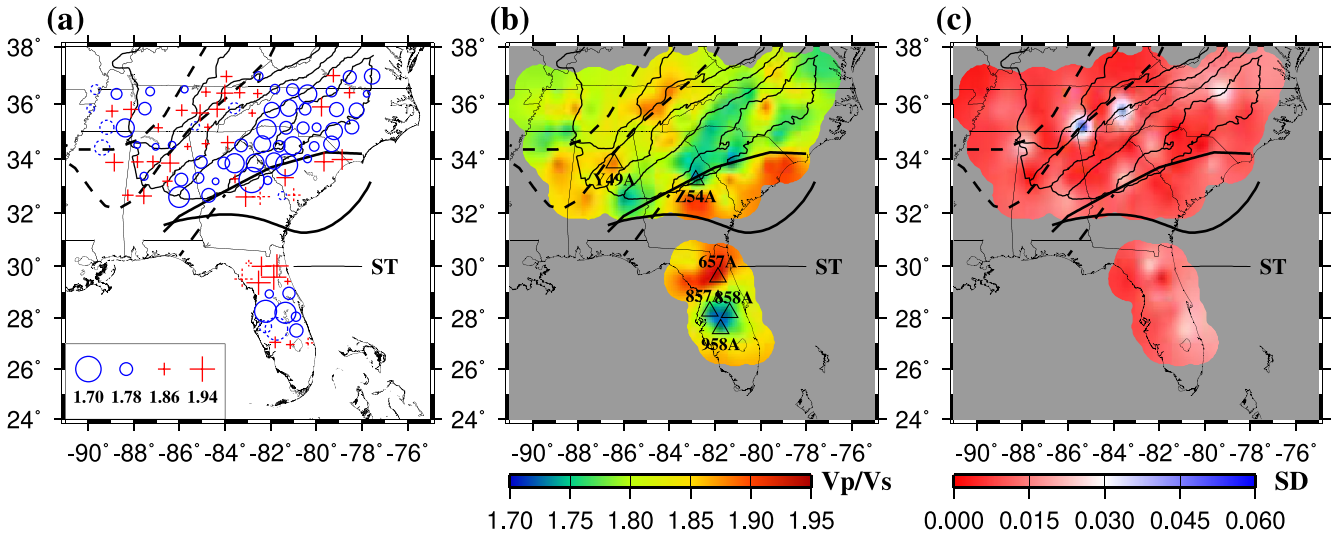

Figure 6. Resulting κ measurements from the H-κ stacking approach. (a) The results are plotted as pluses and circles showing measurements from individual stations. Solid symbols represent measurements provided by stations in Group A, and dashed symbols are for stations in Group B. (b) Spatially smoothed results plotted using a continuous color scale. Triangles show stations discussed in the main text. To generate the spatially continuous data, the discrete data points are fitted using a continuous curvature surface gridding algorithm (Smith & Wessel, 1990) with a tension factor of 0.25 and a spatial interval of 0.1°. Areas that are greater than 1° from the nearest data point are masked. (c) Standard deviation of the resulting κ measurements.

3.3. H Distribution

To generate an H map across the entire study area, we firstly obtain H results from the joint inversion approach for seismic stations in Group A (solid symbols in Figure 7) under the assumption that the Moho is a sharp velocity gradient discontinuity (Shen et al., 2013). We search for the largest velocity gradient within the depth window of 20–60 km of the inverted shear velocity curves underneath each of the stations. We then obtain H values from stations in Group B and Group C, which are marked by the dashed symbols in

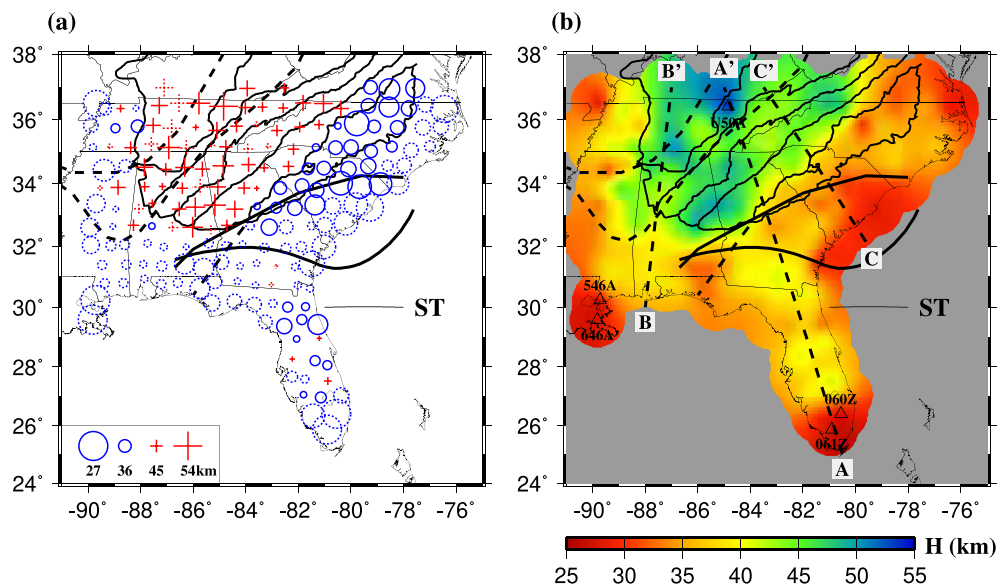

Figure 7. Resulting H measurements. (a) The results are plotted as pluses and circles at the stations. Solid symbols represent H measurements obtained using surface wave and RF joint inversion from stations in Group A, and dashed symbols represent H measurements obtained using surface inversion alone from stations in groups B and C. (b) The results are plotted using a continuous color scale. Parameters used for producing the spatially smoothed data are the same as those used in producing Figure 6b. The three dashed lines show the location of the cross-sections shown in Figure S2 in Supporting Information S1.

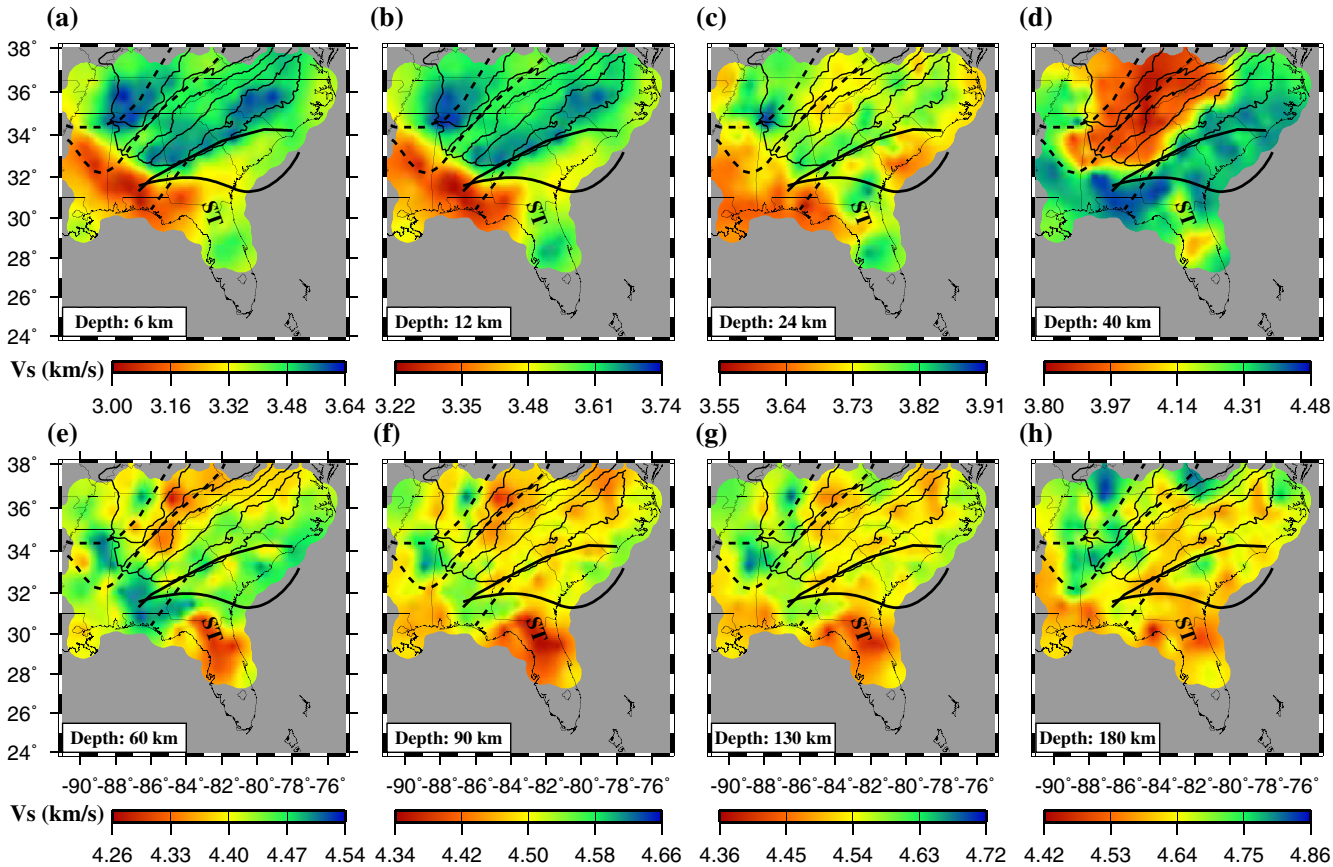

Figure 8. Shear velocity horizontal slices at different depths: (a) 6, (b) 12, (c) 24, (d) 40, (e) 60, (f) 90, (g) 130, and (h) 180 km.

Figure 7, by inverting Rayleigh wave phase velocity dispersions. H values are determined by searching for the largest velocity gradient. Within the entire study area, the resulting H values range from 27.0 km in the southwestern portion of the Gulf Coastal Plain (stations 546A and 646A) and the southern tip of the Suwannee Terrane (stations 060Z and 061Z) to 54.0 km at Station U50A in the northern part of the SAM, within the Grenville Province (Figure 7). The averaged H value computed from all the 186 stations is 39.0 ± 5.8 km. The SAM is characterized by thick crust except for the Carolina Terrane and the Inner Piedmont, and thin crust is mainly found in the Atlantic and Gulf coastal plains. Unlike the κ measurements, no clear changes in H across the Higgins-Zietz Magnetic Boundary are observed.

3.4. Shear Wave Velocities

Due to the unsatisfactory resolution of phase velocity in the southern tip of the Suwannee Terrane (Figure S1 in Supporting Information S1), we did not invert for shear velocities at 9 stations in that area (stations 058A, 059A, 059Z, 060A, 060Z, 061Z, 957A, 958A, and 959A). At the depths of 6 and 12 km (Figures 8a and 8b), the SAM is characterized by high shear wave velocities, while the Gulf Coastal Plain has the lowest shear wave velocities across the entire study area, which are apparently caused by the thick sedimentary layer. The low velocities observed beneath the Gulf Coastal Plain continue downward to the mid-crust (Figure 8c: 24 km), and the high velocities beneath the SAM become more comparable with the rest of the study area at this depth. At 40 km deep (Figure 8d), parts of the Suwannee Terrane and the SAM, with the exception of the Carolina Terrane and the Inner Piedmont, possess relatively low shear velocities. From 60 to 130 km (Figures 8e–8g), a clear low velocity zone is found beneath the northern and central portions of the Suwannee Terrane. At the greatest depth of the velocity model (Figure 8h: 180 km), relatively high velocities are observed beneath the Mazatzal Province and Grenville Province. Figure S2 in Supporting Information S1 shows distributions of H, κ, and Vs along the three profiles shown in Figure 7b.

4. Discussion

4.1. Crustal Modification in the Carolina Terrane and Inner Piedmont

Relative to the average κ value of 1.81 ± 0.05 for the entire SAM, both the Carolina Terrane and Inner Piedmont of the eastern SAM possess lower κ values, ranging from 1.70 to 1.74 (Figure 6), which are consistent with the observations of Parker et al. (2013) obtained along two NW-SE trending profiles and the overall lower than normal κ measurements observed by most other studies (e.g., Ma & Lowry, 2017). The crust has a mean thickness of 35.1 ± 2.7 km in the Carolina Terrane, and 43.0 ± 4.7 km in the Inner Piedmont, which is thinner than that in the Blue Ridge Mountains (45.8 ± 2.3 km) and the Valley and Ridge (45.0 ± 2.1 km). The H measurements obtained from this study are consistent with those from most previous studies (e.g., Buehler & Shearer, 2017; Shen & Ritzwoller, 2016), but for the Blue Ridge Mountains, they are smaller than the >50 km thickness obtained along two dense profiles traversing the SAM (Hopper et al., 2016). The main cause of the differences is the crustal velocities used to obtain the H values, as demonstrated in Buehler and Shearer (2017). The Vs values in the lowermost 10 km layer of the crust beneath the Carolina Terrane are slightly higher than the Vs value of 3.75 km/s for the lower crust in the IASP91 earth model, and those observed in the Inner Piedmont are the highest among all the subareas of the SAM (Figure 9). These observations are in general agreement with those obtained by the continental-scale study of Shen and Ritzwoller (2016).

Based on the tectonic history of the area and the H, κ, and Vs measurements, in the following we discuss two processes that might be responsible for the observations. The first is the complete loss of the original lower continental crust through delamination, which is the process of decoupling of the continental lower crust and upper mantle from the overlying upper crust (Bird, 1979; Kay & Kay, 1991; Meissner & Mooney, 1998). The metamorphic transition from gabbro to denser eclogite in the lowermost crust plays the major role in producing the negative buoyancy needed for delamination (Rey, 1993). The required high temperature (>∼500°C) and high pressure (>∼1.2 GPa) conditions are commonly found in arcs and other tectonically active environments such as continental rifts and volcanic rifted margins (Jull & Kelemen, 2001). Since the Carolina Terrane was a volcanic island arc accreted on to the Inner Piedmont shortly prior to the assembly of Pangaea (Hatcher et al., 1989), lower crustal delamination is a possible mechanism to produce the observed felsic crustal composition. However, because the average continental upper crust is only 20–25 km thick (as indicated by most standard earth models such as the IASP91), in order to produce the ∼35–45 km post-delamination crust, a doubling in crustal thickness is required either before or after the delamination. Such a significant crustal thickening is not commonly observed in island arcs. Another problem with this model is that the observed Vs values in the lowermost crustal layer beneath the Carolina Terrane and the Inner Piedmont are both higher than the Vs of 3.75 km/s for normal lower continental crust (Figure 9). Additionally, because the Carolina Terrane was closer to the convergent boundary than the Inner Piedmont, one would expect that crustal shortening would be more extensive in the former area than the latter, leading to a thicker crust in the former area which contradicts the observations (Figure 7). Therefore, it is unlikely that the entire crust is composed of the thickened original felsic upper crust.

The second and our preferred model is that the original mafic lower continental crust beneath oceanic island arcs was replaced by silica-rich materials originated from the subducted oceanic slab, a process termed relamination (Hacker et al., 2011). The mantle-derived felsic relaminated layer is expected to have a κ value that is comparable to that of the upper crust, leading to the observed low κ values beneath the Carolina Terrane and the Inner Piedmont (Figure 6b). The final crustal thickness is dependent on the thickness of the original upper crust and that of the relaminated layer. However, although the relaminated layer is expected to have higher seismic velocities than the upper crust, whether they are higher than the lower crustal Vs in the IASP91 earth model is unknown. This relamination model for the Inner Piedmont has also been advocated by Parker et al. (2013), who attribute the relamination process to continental collision initiated at ca. 1,190 Ma during the Proterozoic Grenville orogeny (Rivers & Corrigan, 2000).

4.2. Lithospheric Evolution Beneath the Suwannee Terrane

The Suwannee Terrane has been recognized as being exotic to North America by Wilson (1966), with the Brunswick Magnetic Anomaly being generally considered to be the northern boundary of the terrane. The

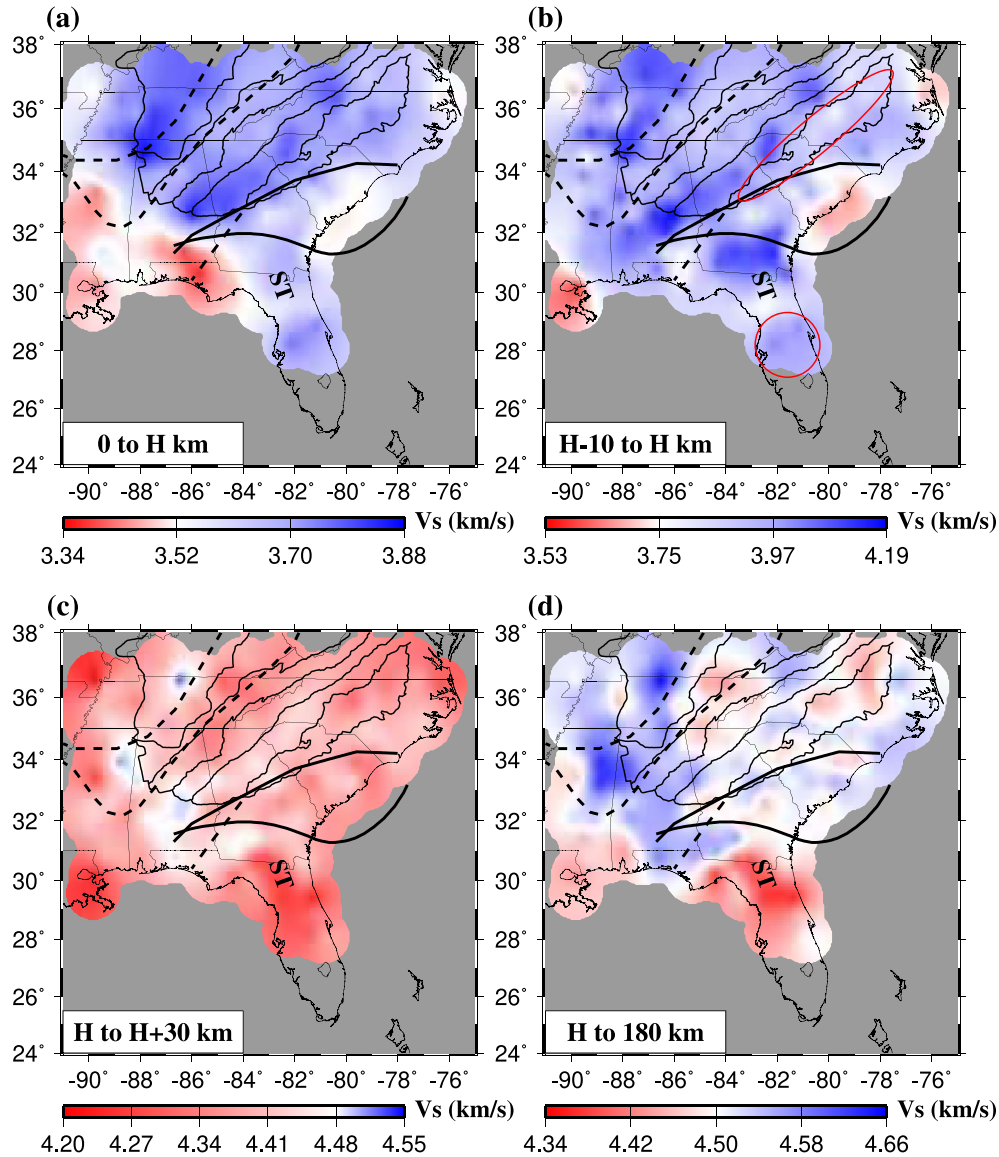

Figure 9. Mean shear wave velocities for different depth ranges. (a) The entire crust. (b) The lowermost 10-km-thick layer of the crust. Areas enclosed by the red ellipses are possible locations for crustal delamination/relamination. (c) The uppermost 30-km-thick layer of the mantle. (d) From the Moho to 180 km deep. For each plot, the white color indicates the mean Vs in the IASP91 velocity model for the corresponding layer. ST: Suwannee Terrene.

Suwannee Terrane is characterized by high κ values with the exception of the central portion, which is largely occupied by the Osceola intrusive complex (e.g., Boote et al., 2018). The overall high κ values (averaged 1.83 ± 0.07 for the whole area, and 1.85 ± 0.05 without the central portion; Figure 6b) can be attributed to a number of tectonic-magmatic events such as the placement of the Central Atlantic Magmatic Province during the breakup of Pangaea in Late Triassic and Early Jurassic (Nomade et al., 2007; Wagner et al., 2018; Whalen et al., 2015), Late Triassic rifting that created the Georgia Basin (McBride, 1991), and magmatism (625 - 550 Ma) during the subduction of the Osceola Arc (Boote et al., 2018).

The mean κ value computed from the three stations located in the central Suwannee Terrane (Figure 6b) is 1.72 ± 0.01 (1.72 at 857A, 1.73 at 858A, and 1.72 at 958A), which is lower than the global average of 1.78 for continental crust (Christensen, 1996). In addition, a high shear wave velocity layer at the bottom of the crust beneath this area is observed, with a mean shear velocity for the 10-km-thick layer atop the Moho of ~4.0 km/s which is ~6.5% higher than the corresponding value in the IASP91 model (Figure 9b). These

characteristics are comparable to the Carolina Terrane discussed above, where lower crustal eclogitization and delamination followed by relamination are proposed as a viable formation mechanism.

In the uppermost mantle beneath the northern Suwannee Terrane, a distinct low velocity anomaly is found from ~60 km to the depth of 180 km (Figures 8e–8h). This low velocity anomaly has also been observed by other tomography studies (e.g., Biryol et al., 2016; Pollitz & Mooney, 2016; Shen & Ritzwoller, 2016; Wagner et al., 2018), although some tomography studies show that the low velocity anomaly extends deeper than 180 km (e.g., Biryol et al., 2016; Schmandt & Lin, 2014; Wagner et al., 2018). Shen and Ritzwoller (2016) also observe a lower velocity anomaly at approximately the same location at the depths of 70, 90, and 120 km. This area spatially coincides with an area with a shallow lithosphere-asthenosphere boundary relative to the rest of the Suwannee Terrane (Figure 2a; Hopper & Fischer, 2018; Liu & Gao, 2018; Pasyanos et al., 2014). While this spatial correspondence between the thin lithosphere and low mantle velocities could be accidental, additional observational and modeling studies may lead to a better understanding of the processes responsible for the lithospheric thinning and low mantle velocities.

Another interesting question that deserves additional study is the nature of the Higgins-Zietz Magnetic Boundary (Higgins & Zietz, 1983; Williams & Hatcher, 1982). While most of the surface tectonic boundaries in the study area correspond well with lateral variations in shear wave velocities and crust H and κ measurements (Figures 6–8), the Higgins-Zietz Magnetic Boundary, which bisects the Atlantic Coastal Plain in the study area (Figure 1), does not correspond to clear changes in H and Vs, but is a clear boundary of κ measurements, suggesting that it is a boundary of crustal blocks with different composition and/or physical states. Whether such a change reflects the difference in the original Gondwana/Laurentia crust, or a difference in the degree of crustal modification by more recent events such as the opening of the Atlantic Ocean, can only be resolved by additional interdisciplinary studies.

4.3. Magmatic Intrusion Underneath the Grenville Province

The Grenville Province and a narrow zone adjacent to its eastern boundary are characterized by higher-than-normal κ values compared to the neighboring areas (Figure 6). Most κ values in the area are larger than 1.85 with the largest value of 1.90 found at Station Y49A near the southeastern part of the area (Figure 6). Overall high κ values in the Grenville Province are also revealed by Ma and Lowry (2017). A recent study by Stein et al. (2018) proposes that the Grenville Province in the central United States, extending from Michigan to Alabama, is a part of the eastern arm of the Proterozoic Midcontinent Rift. Magmatic rocks observed in the rift system along with the seismic reflection evidence suggest possible existence of lower crustal magmatic intrusion and uppermost mantle magmatic underplating associated with crustal extension (e.g., Behrendt et al., 1990). In the Grenville Province and the narrow zone to the east, a large amount of mafic rocks have been found (Misra & McSween, 1984), which correlates well with our observed high κ values. High κ values related with active rifting have also been observed in other segments of the Midcontinent Rift (e.g., Moidaki et al., 2013; Zhang et al., 2016). Therefore, we speculate that magmatic intrusion associated with the Proterozoic rifting might be the major reason for the higher-than-normal κ measurements observed in this area.

5. Conclusions

By jointly inverting RFs and Rayleigh wave phase velocity dispersion computed from ambient noise and teleseismic data, we have imaged crustal and upper mantle structure in the top 180 km beneath the southeastern United States. Our results are consistent with the hypothesis that the Carolina Terrane and Inner Piedmont in the eastern Southern Appalachian Mountains, and possibly the central Suwannee Terrane, have undergone delamination/relamination, as evidenced by the low κ and slow lowermost crustal velocities relative to the western part of the Southern Appalachian Mountains. The Grenville Province and adjacent areas are characterized by elevated κ measurements, which can be attributed to magmatic intrusion during the period of extension of the Proterozoic Midcontinent Rift. Additional investigations are needed to explore possible links between the anomalous thin lithosphere and low seismic velocities beneath the northern Suwannee Terrane, and the nature of the Higgins-Zietz Magnetic Boundary.

Data Availability Statement

All the data used to derive the measurements presented above are publicly available, under the network code of TA (https://doi.org/10.7914/SN/TA), from the Incorporated Research Institutions for Seismology Data Management Center using the BREQ_FAST request procedure which is detailed in https://ds.iris.edu/ds/nodes/dmchttp://ds.iris.edu/ds/nodes/dmc/forms/breqfast-request (last accessed: October, 2018).

Acknowledgments
Constructive comments from two anonymous reviewers and the Associate Editor greatly improved the manuscript. The study was partially supported by the American Chemical Society under grant PRF-60281-ND8, and the U.S. National Science Foundation under award 1919789.

References

Aleinikoff, J. N., Zartman, R. E., Walter, M., Rankin, D. W., Lyttle, P. T., & Burton, W. C. (1995). U-Pb ages of metarhyolites of the Catoctin and Mount Rogers formations, Central and Southern Appalachians: Evidence for two pulses of Iapetan rifting. *American Journal of Science*, *295*(4), 428–454. https://doi.org/10.2475/ajs.295.4.428

Ammon, C. J., Randall, G. E., & Zandt, G. (1990). On the nonuniqueness of receiver function inversions. *Journal of Geophysical Research*, *95*(B10), 15303–15318. https://doi.org/10.1029/JB095iB10p15303

Behrendt, J. C., Hutchinson, D. R., Lee, M., Thornber, C. R., Trehu, A., Cannon, W., & Green, A. (1990). GLIMPCE Seismic reflection evidence of deep-crustal and upper-mantle intrusions and magmatic underplating associated with the Midcontinent Rift system of North America. *Tectonophysics*, *173*(1–4), 595–615. https://doi.org/10.1016/0040-1951(90)90248-7

Bensen, G. D., Ritzwoller, M. H., & Shapiro, N. M. (2008). Broadband ambient noise surface wave tomography across the United States. *Journal of Geophysical Research*, *113*(B5), B05306. https://doi.org/10.1029/2007JB005248

Bird, P. (1979). Continental delamination and the Colorado Plateau. *Journal of Geophysical Research*, *84*(B13), 7561–7571. https://doi.org/10.1029/JB084iB13p07561

Biryol, C. B., Wagner, L. S., Fischer, K. M., & Hawman, R. B. (2016). Relationship between observed upper mantle structures and recent tectonic activity across the Southeastern United States. *Journal of Geophysical Research: Solid Earth*, *121*, 3393–3414. https://doi.org/10.1002/2015JB012698

Boote, S. K., & Knapp, J. H. (2016). Offshore extent of Gondwanan Paleozoic strata in the southeastern United States: The Suwannee suture zone revisited. *Gondwana Research*, *40*, 199–210. https://doi.org/10.1016/j.gr.2016.08.011

Boote, S. K., Knapp, J. H., & Mueller, P. A. (2018). Preserved Neoproterozoic continental collision in Southeastern North America: The Brunswick Suture Zone and Osceola continental margin Arc. *Tectonics*, *37*(1), 305–321. https://doi.org/10.1002/2017TC004732

Buehler, J. S., & Shearer, P. M. (2017). Uppermost mantle seismic velocity structure beneath USArray. *Journal of Geophysical Research: Solid Earth*, *122*, 436–448. https://doi.org/10.1002/2016JB013265

Christensen, N. I. (1996). Poisson's ratio and crustal seismology. *Journal of Geophysical Research: Solid Earth*, *101*(B2), 3139–3156. https://doi.org/10.1029/95JB03446

Clayton, R. W., & Wiggins, R. A. (1976). Source shape estimation and deconvolution of teleseismic bodywaves. *Geophysical Journal International*, *47*(1), 151–177. https://doi.org/10.1111/j.1365-246X.1976.tb01267.x

Cunningham, E., & Lekic, V. (2019). Constraining crustal structure in the presence of sediment: A multiple converted wave approach. *Geophysical Journal International*, *219*(1), 313–327. https://doi.org/10.1093/gji/ggz298

Cunningham, E., & Lekic, V. (2020). Constraining properties of sedimentary strata using receiver functions: An example from the Atlantic Coastal Plain of the southeastern United States. *Bulletin of the Seismological Society America*, *110*(2), 519–533. https://doi.org/10.1785/0120190191

Dennis, A. J., & Wright, J. E. (1997). The Carolina terrane in northwestern South Carolina, U.S.A.: Late Precambrian-Cambrian deformation and metamorphism in a peri-Gondwanan oceanic arc. *Tectonics*, *16*(3), 460–473. https://doi.org/10.1029/97TC00449

Dziewonski, A., Bloch, S., & Landisman, M. (1969). A technique for the analysis of transient seismic signals. *Bulletin of the Seismological Society of America*, *59*(1), 427–444. https://doi.org/10.1785/bssa0590010427

Dziewonski, A. M., & Anderson, D. L. (1981). Preliminary reference Earth model. *Physics of the Earth and Planetary Interiors*, *25*(4), 297–356. https://doi.org/10.1016/0031-9201(81)90046-7

Efron, B., & Tibshirani, R. (1986). Bootstrap methods for standard errors, confidence intervals, and other measures of statistical accuracy. *Statistical Science*, *1*(1), 54–75. https://doi.org/10.1214/ss/1177013815

Fischer, K. M. (2002). Waning buoyancy in the crustal roots of old mountains. *Nature*, *417*(6892), 933–936. https://doi.org/10.1038/nature00855

Gaite, B., Iglesias, A., Villasenor, A., Herraiz, M., & Pacheco, J. F. (2012). Crustal structure of Mexico and surrounding regions from seismic ambient noise tomography. *Geophysical Journal International*, *188*(3), 1413–1424. https://doi.org/10.1111/j.1365-246X.2011.05339.x

Gao, S. S., & Liu, K. H. (2012). AnisDep: A FORTRAN program for the estimation of the depth of anisotropy using spatial coherency of shear-wave splitting parameters. *Computers & Geosciences*, *49*, 330–333. https://doi.org/10.1016/j.cageo.2012.01.020

Gao, S. S., & Liu, K. H. (2014). Mantle transition zone discontinuities beneath the contiguous United States. *Journal of Geophysical Research: Solid Earth*, *119*, 452–6468. https://doi.org/10.1002/2014JB011253

Golos, E., Fang, H., & van der Hilst, R. D. (2020). Variations in seismic wave speed and Vp/Vs ratio in the North American lithosphere. *Journal of Geophysical Research: Solid Earth*, *125*(12), e2020JB020574. https://doi.org/10.1029/2020JB020574

Hacker, B. R., Kelemen, P. B., & Behn, M. D. (2011). Differentiation of the continental crust by relamination. *Earth and Planetary Science Letters*, *307*(3–4), 501–516. https://doi.org/10.1016/j.epsl.2011.05.024

Hatcher, R. D., Thomas, W. A., Geiser, P. A., Snoke, A. W., Mosher, S., & Wiltschko, D. V. (1989). Alleghanian orogen. In R. D. Hatcher, W. A. Thomas, & G. W. Viele (Eds.), *The Appalachian-Ouachita Orogen in the United States* (Vol. F-2, pp. 233–318). Boulder, Colorado: Geological Society of America.

Hawman, R. B., Khalifa, M. O., & Baker, M. S. (2012). Isostatic compensation for a portion of the Southern Appalachians: Evidence from a reconnaissance study using wide-angle, three-component seismic soundings. *Geological Society of America Bulletin*, *124*(3–4), 291–317. https://doi.org/10.1130/B30464.1

Heatherington, A. L., & Mueller, P. A. (2003). Mesozoic igneous activity in the Suwannee terrane, southeastern USA: Petrogenesis and Gondwanan affinities. *Gondwana Research*, *6*(2), 296–311. https://doi.org/10.1016/S1342-937X(05)70979-5

Higgins, M. W., & Zietz, I. (1983). Geologic interpretation of geophysical maps of the pre-Cretaceous "basement" beneath the coastal plain of the southeastern United States. *Geological Society of America Memoirs*, *158*, 125–130. https://doi.org/10.1130/MEM158-p125

Hopper, E., & Fischer, K. M. (2018). The changing face of the Lithosphere-Asthenosphere boundary: Imaging continental scale patterns in upper mantle structure across the contiguous U.S. with Sp converted waves. *Geochemistry, Geophysics, Geosystems*, *19*(8), 2593–2614. https://doi.org/10.1029/2018GC007476

Hopper, E., Fischer, K. M., Rondenay, S., Hawman, R. B., & Wagner, L. S. (2016). Imaging crustal structure beneath the southern Appalachians with wavefield migration. *Geophysical Research Letters*, *43*, 12054–12062. https://doi.org/10.1002/2016GL071005

Hopper, E., Fischer, K. M., Wagner, L. S., & Hawman, R. B. (2017). Reconstructing the end of the Appalachian orogeny. *Geology*, *45*(1), 15–18. https://doi.org/10.1130/G38453.1

Iverson, W. P., & Smithson, S. B. (1983). Reprocessing and reinterpretation of COCORP southern Appalachian profiles. *Earth and Planetary Science Letters*, *62*(1), 75–90. https://doi.org/10.1016/0012-821X(83)90072-9

Jull, M., & Kelemen, P. B. (2001). On the conditions for lower crustal convective instability. *Journal of Geophysical Research*, *106*(B4), 6423–6446. https://doi.org/10.1029/2000JB900357

Kanamori, H., & Anderson, D. L. (1977). Importance of physical dispersion in surface wave and free oscillation problems: Review. *Reviews of Geophysics*, *15*(1), 105–112. https://doi.org/10.1029/RG015i001p00105

Kay, R. W., & Kay, S. (1991). Creation and destruction of lower continental crust. *Geologische Rundschau*, *80*(2), 259–278. https://doi.org/10.1007/BF01829365

Kean, A. E., & Long, L. T. (1980). A seismic refraction line along the axis of the southern Piedmont and crustal thicknesses in the southeastern United States. *Seismological Research Letters*, *51*(4), 3–14. https://doi.org/10.1785/gssrl.51.4.3

Kennett, B. L. N., & Engdahl, E. R. (1991). Traveltimes for global earthquake location and phase identification. *Geophysical Journal International*, *105*(2), 429–465. https://doi.org/10.1111/j.1365-246X.1991.tb06724.x

Langston, C. A. (2011). Wave-field continuation and decomposition for passive seismic imaging under deep unconsolidated sediments. *Bulletin of the Seismological Society America*, *101*(5), 2176–2190. https://doi.org/10.1785/0120100299

Laske, G., & Masters, G. (1997). A global digital map of sediment thickness. EOS Transaction American Geophysical Union. (Vol. 78, p. F483).

Laske, G., Masters, G., Ma, Z., & Pasyanos, M. (2013). Update on CRUST1.0 - A 1-degree global model of Earth's crust. *Geophysical Research Abstracts*, *15*. Abstract EGU2013-2658.

Li, C., Gao, H., & Williams, M. L. (2020). Seismic characteristics of the eastern North American crust with Ps converted waves: Terrane accretion and modification of continental crust. *Journal of Geophysical Research: Solid Earth*, *125*(5), e2019JB018727. https://doi.org/10.1029/2019JB018727

Liu, K. H., & Gao, S. S. (2010). Spatial variations of crustal characteristics beneath the Hoggar swell, Algeria, revealed by systematic analyses of receiver functions from a single seismic station. *Geochemistry, Geophysics, Geosystems*, *11*(8), Q08011. https://doi.org/10.1029/2010GC003091

Liu, L., & Gao, S. S. (2018). Lithospheric layering beneath the contiguous United States constrained by S-to-P receiver functions. *Earth and Planetary Science Letters*, *495*, 79–86. https://doi.org/10.1016/j.epsl.2018.05.012

Liu, L., Gao, S. S., Liu, K. H., & Mickus, K. (2017). Receiver function and gravity constraints on crustal structure and vertical movements of the Upper Mississippi Embayment and Ozark Uplift. *Journal of Geophysical Research: Solid Earth*, *122*(6), 4572–4583. https://doi.org/10.1002/2017JB014201

Liu, T., & Shearer, P. M. (2021). Complicated lithospheric structure beneath the contiguous US revealed by teleseismic S-reflections. *Journal of Geophysical Research: Solid Earth*, *126*, e2020JB021624. https://doi.org/10.1029/2020JB021624

Loewy, S. L., Connelly, J. N., Dalziel, I. W. D., & Gower, C. F. (2003). Eastern Laurentia in Rodinia: Constraints from whole-rock Pb and U/Pb geochronology. *Tectonophysics*, *375*(1–4), 169–197. https://doi.org/10.1016/S0040-1951(03)00338-X

Ma, X., & Lowry, A. R. (2017). USArray imaging of continental crust in the Conterminous United States. *Tectonics*, *36*(12), 2882–2902. https://doi.org/10.1002/2017TC004540

MacDougall, J. G., Fischer, K. M., Forsyth, D. W., Hawman, R. B., & Wagner, L. S. (2015). Shallow mantle velocities beneath the southern Appalachians from Pn phases. *Geophysical Research Letters*, *42*, 339–345. https://doi.org/10.1002/2014GL062714

Marzen, R. E., Shillington, D. J., Lizarralde, D., & Harder, S. H. (2019). Constraints on Appalachian orogenesis and continental rifting in the southeastern United States from wide-angle seismic data. *Journal of Geophysical Research: Solid Earth*, *124*(7), 6625–6652. https://doi.org/10.1029/2019JB017611

Marzoli, A., Renne, P. R., Piccirillo, E. M., Ernesto, M., Bellieni, G., & De Min, A. (1999). Extensive 200-million-year-old continental flood basalts of the Central Atlantic Magmatic Province. *Science*, *284*(5414), 616–618. https://doi.org/10.1126/science.284.5414.616

McBride, J. H. (1991). Constraints on the structure and tectonic development of the Early Mesozoic South Georgia Rift, southeastern United States; Seismic reflection data processing and interpretation. *Tectonics*, *10*(5), 1065–1083. https://doi.org/10.1029/90TC02682

McBride, J. H., & Nelson, K. D. (1988). Integration of COCORP deep reflection and magnetic anomaly analysis in the southeastern United States: Implications for origin of the Bruns- wick and East Coast magnetic anomalies. *Geological Society of America Bulletin*, *100*(3), 436–445. https://doi.org/10.1130/0016-7606(1988)100<0436:IOCDRA>2.3.CO;2

McGlannan, A. J., & Gilbert, H. (2016). Crustal signatures of the tectonic development of the North American midcontinent. *Earth and Planetary Science Letters*, *43*(1), 339–349. https://doi.org/10.1016/j.epsl.2015.10.048

Meissner, R., & Mooney, W. (1998). Weakness of the lower continental crust: A condition for delamination, uplift, and escape. *Tectonophysics*, *296*(1–2), 47–60. https://doi.org/10.1016/S0040-1951(98)00136-X

Misra, K. C., & McSween, H. Y. (1984). Mafic rocks of the Southern Appalachians: A review. *American Journal of Science*, *284*(4–5), 294–318. https://doi.org/10.2475/ajs.284.4-5.294

Moidaki, M., Gao, S. S., Liu, K. H., & Atekwana, E. (2013). Crustal thickness and Moho sharpness beneath the Midcontinent Rift from receiver functions. *Research in Geophysics*, *3*(1). https://doi.org/10.4081/rg.2013.e1

Nair, S. K., Gao, S. S., Liu, K. H., & Silver, P. G. (2006). Southern African crustal evolution and composition: Constraints from receiver function studies. *Journal of Geophysical Research*, *111*(B2), B02304. https://doi.org/10.1029/2005JB003802

Nelson, K. D., Arnow, J. A., McBride, J. H., Willemin, J. H., Huang, J., Zheng, L., et al. (1985). New COCORP profiling in the southeastern United States. Part I: Late Paleozoic suture and Mesozoic rift basin. *Geology*, *13*(10), 714–718. https://doi.org/10.1130/0091-7613(1985)13<714:NCPITS>2.0.CO;2

Netto, A., & Pulliam, J. (2020). Upper mantle structure of the southern U.S. continental margin from teleseismic traveltime tomography. *Geophysical Research Letters*, *47*, e2019GL085482. https://doi.org/10.1029/2019GL085482

Nomade, S., Knight, K. B., Beutel, E., Renne, P. R., Verati, C., Feraud, G., et al. (2007). Chronology of the Central Atlantic Magmatic Province: Implications for the Central Atlantic rifting processes and the Triassic-Jurassic biotic crisis. *Palaeogeography, Palaeoclimatology, Palaeoecology*, *244*(1–4), 326–344. https://doi.org/10.1016/j.palaeo.2006.06.034

Owens, B. E., & Tucker, R. D. (2003). Geochronology of the Mesoproterozoic State Farm gneiss and associated Neoproterozoic granitoids, Goochland terrane, Virginia. *Geological Society of America Bulletin*, *115*(8), 972–982. https://doi.org/10.1130/B25258.1

Parker, E. H., Hawman, R. B., Fischer, K. M., & Wagner, L. S. (2013). Crustal evolution across the southern Appalachian: Initial results from the SESAME broadband array. *Geophysical Research Letters*, *40*(15), 3853–3857. https://doi.org/10.1002/grl.50761

Pasyanos, M. E., Masters, T. G., Laske, G., & Ma, Z. (2014). LITHO1.0: An updated crust and lithospheric model of the Earth. *Journal of Geophysical Research: Solid Earth*, *119*, 2153–2173. https://doi.org/10.1002/2013JB010626

Pollitz, F. F., & Mooney, W. F. (2016). Seismic velocity structure of the crust and shallow mantle of the Central and Eastern United States by seismic surface wave imaging. *Geophysical Research Letters*, *43*(1), 118–126. https://doi.org/10.1002/2015GL066637

Porter, R., Liu, Y., & Holt, W. E. (2016). Lithospheric records of orogeny within the continental U.S. *Geophysical Research Letters*, *43*, 144–153. https://doi.org/10.1002/2015GL066950

Prodehl, C., Schlittenhardt, J., & Stewart, S. W. (1984). Crustal structure of the Appalachian Highlands in Tennessee. *Tectonophysics*, *109*(1–2), 61–76. https://doi.org/10.1016/0040-1951(84)90170-7

Rey, P. (1993). Seismic and tectono-metamorphic characters of the lower continental crust in Phanerozoic areas: A consequence of post-thickening extension. *Tectonics*, *12*(2), 580–590. https://doi.org/10.1029/92TC01568

Rivers, T., & Corrigan, D. (2000). Convergent margin on southeastern Laurentia during the Mesoproterozoic: Tectonic implications. *Canadian Journal of Earth Sciences*, *37*(2–3), 359–383. https://doi.org/10.1139/e99-067

Rogers, J. J. W., & Santosh, M. (2003). Supercontinents in Earth history. *Gondwana Research*, *6*(3), 357–368. https://doi.org/10.1016/S1342-937X(05)70993-X

Schlische, R. W. (1993). Anatomy and evolution of the Triassic-Jurassic Continental Rift System, eastern North America. *Tectonics*, *12*(4), 1026–1042. https://doi.org/10.1029/93TC01062

Schmandt, B., & Lin, F.-C. (2014). P and S wave tomography of the mantle beneath the United States. *Geophysical Research Letters*, *41*(18), 6342–6349. https://doi.org/10.1002/2014GL061231

Shen, W., & Ritzwoller, M. H. (2016). Crustal and uppermost mantle structure beneath the United States. *Journal of Geophysical Research: Solid Earth*, *121*, 4306–4342. https://doi.org/10.1002/2016JB012887

Shen, W., Ritzwoller, M. H., Schulte-Pelkum, V., & Lin, F.-C. (2013). Joint inversion of surface wave dispersion and receiver functions: A Bayesian Monte-Carlo approach. *Geophysical Journal International*, *192*(2), 807–836. https://doi.org/10.1093/gji/ggs050

Shrivastava, A., Liu, K. H., & Gao, S. S. (2021). Teleseismic P-wave attenuation beneath the southeastern United States. *Geochemistry, Geophysics, Geosystems*, *22*(6), e2021GC009715. https://doi.org/10.1029/2021GC009715

Smith, W. H. F., & Wessel, P. (1990). Gridding with continuous curvature splines in tension. *Geophysics*, *55*(3), 293–305. https://doi.org/10.1190/1.1442837

Spica, Z., Perton, M., Calo, M., Legrand, D., Cordoba-Montiel, F., & Iglesias, A. (2016). 3-D shear wave velocity model of Mexico and South US: Bridging seismic networks with ambient noise cross-correlations (c^1) and correlation of coda of correlations (c^3). *Geophysical Journal International*, *206*(3), 795–1813. https://doi.org/10.1093/gji/ggw240

Stein, C. A., Stein, S., Elling, R., Keller, G. R., & Kley, J. (2018). Is the "Grenville Front" in the central United States really the Midcontinent Rift? *Geological Society of America Today*, *28*(5), 4–10. https://doi.org/10.1130/GSATG357A.1

Thomas, W. A. (2006). Tectonic inheritance at a continental margin. *Geological Society of America Today*, *16*(2), 4–11. https://doi.org/10.1130/1052-5173(2006)016[4:TIAACM]2.0.CO;2

Tohver, E., Bettencourt, J. S., Tosdal, R., Mezger, K., Leite, W. B., & Payolla, B. L. (2004). Terrane transfer during the Grenville orogeny: Tracing the Amazonian ancestry of southern Appalachian basement through Pb and Nd isotopes. *Earth and Planetary Science Letters*, *228*(1–2), 161–176. https://doi.org/10.1016/j.epsl.2004.09.029

Verellen, D. N., Alberts, E. C., Larramendi, G. A., Parker, E. H., Jr, & Hawman, R. B. (2020). P-wave reflectivity of the crust and upper mantle beneath the southern Appalachians and Atlantic coastal plain using global phases. *Geophysical Research Letters*, *47*(18), e2020GL089648. https://doi.org/10.1029/2020GL089648

Wagner, L. S., Fischer, K. M., Hawman, R., Hopper, E., & Howell, D. (2018). The relative roles of inheritance and long-term passive margin lithospheric evolution on the modern structure and tectonic activity in the southeastern United States. *Geosphere*, *14*(4), 1385–1410. https://doi.org/10.1130/GES01593.1

Wang, H., Zhao, D., Huang, Z., & Wang, L. (2019). Tomography, seismotectonics, and mantle dynamics of Central and Eastern United States. *Journal of Geophysical Research: Solid Earth*, *124*(8), 8907. https://doi.org/10.1029/2019JB017478

Wang, T., Feng, J., Liu, K. H., & Gao, S. S. (2019). Crustal structure beneath the Malawi and Luangwa Rift Zones and adjacent areas from ambient noise tomography. *Gondwana Research*, *67*, 187–198. https://doi.org/10.1016/j.gr.2018.10.018

Wang, T., Gao, S. S., Dai, Y., Yang, Q., & Liu, K. H. (2019). Lithospheric structure and evolution of southern Africa: Constrains from joint inversion of Rayleigh wave dispersion and receiver functions. *Geochemistry, Geophysics, Geosystems*, *20*(7), 3311–3327. https://doi.org/10.1029/2019GC008259

Whalen, L., Gazel, E., Vidito, C., Puffer, J., Bizimis, M., Henika, W., & Caddick, M. J. (2015). Supercontinental inheritance and its influence on supercontinental breakup: The Central Atlantic Magmatic Province and the breakup of Pangea. *Geochemistry, Geophysics, Geosystems*, *16*(10), 3532–3554. https://doi.org/10.1002/2015GC005885

Whitmeyer, S. J., & Karlstrom, K. E. (2007). Tectonic model for the Proterozoic growth of North America. *Geosphere*, *3*(4), 220–259. https://doi.org/10.1130/GES00055.1

Williams, H., & Hatcher, R. D. (1982). Suspect terranes and accretionary history of the Appalachian orogen. *Geology*, *10*(10), 530–536. https://doi.org/10.1130/0091-7613(1982)10<530:STAAHO>2.0.CO;2

Wilson, J. T. (1966). Did the Atlantic close and then re-open? *Nature*, *211*(5050), 676–681. https://doi.org/10.1038/211676a0

Yang, Y., Li, A., & Ritzwoller, M. H. (2008). Crustal and uppermost mantle structure in southern Africa revealed from ambient noise and teleseismic tomography. *Geophysical Journal International*, *174*(1), 235–248. https://doi.org/10.1111/j.1365-246X.2008.03779.x

Yao, H., van der Hilst, R. D., & de Hoop, M. V. (2006). Surface-wave array tomography in SE Tibet from ambient seismic noise and two-station analysis - I. Phase velocity maps. *Geophysical Journal International*, *166*(2), 732–744. https://doi.org/10.1111/j.1365-246X.2006.03028.x

Yu, Y., Song, J., Liu, K. H., & Gao, S. S. (2015). Determining crustal structure beneath seismic stations overlying a low-velocity sedimentary layer using receiver functions. *Journal of Geophysical Research: Solid Earth*, *120*, 3208–3218. https://doi.org/10.1002/2014JB011610

Yuan, H., French, S., Cupillard, P., & Romanowicz, B. (2014). Lithospheric expression of geological units in central and eastern North America from full waveform tomography. *Earth and Planetary Science Letters*, *402*(C), 176–186. https://doi.org/10.1016/j.epsl.2013.11.057

Zelt, B. C., & Ellis, R. M. (1999). Receiver-function studies in the Trans-Hudson Orogen, Saskatchewan. *Canadian Journal of Earth Sciences*, *36*(4), 585–603. https://doi.org/10.1139/e98-109

Zhang, H., van der Lee, S., Wolin, E., Bollmann, T. A., Revenaugh, J., Wiens, D. A., et al. (2016). Distinct crustal structure of the North American Midcontinent Rift from P wave receiver functions. *Journal of Geophysical Research: Solid Earth*, *121*, 8136–8153. https://doi.org/10.1002/2016JB013244

Zhang, H. L., Ravat, D., & Lowry, A. R. (2020). Crustal composition and Moho variations of the central and eastern United States: Improving resolution and geologic interpretation of EarthScope USArray seismic images using gravity. *Journal of Geophysical Research: Solid Earth*, *125*, e2019JB018537. https://doi.org/10.1029/2019JB018537

Zhu, L., & Kanamori, H. (2000). Moho depth variation in southern California from teleseismic receiver functions. *Journal of Geophysical Research*, *105*(B2), 2969–2980. https://doi.org/10.1029/1999JB900322